QCD AT COLLIDERS

R. HIROSKY
University of Virginia, Dept. of Physics, Charlottesville, VA 22904, USA
E-mail: hirosky@virginia.edu

The success of the theory of Quantum Chromodynamics (QCD) in describing processes controlled by the strong interaction is generally seen as a triumph of modern particle physics. This paper reviews recent QCD measurements using hadronic jet final states from the Fermilab Tevatron, DESY's HERA, and CERN's LEP colliders. Recent advancements in the measurements of jet production cross sections, events shapes, and energy flow, along with improved theoretical calculations, allow for new levels of precision in the study of the physics of strong interactions and point to areas in need of further refinement.

1. Introduction

In the framework of quantum chromodynamics (QCD) outgoing hadronic jets are a key signature of strong interactions between constituent partons in inelastic hadron collisions. We have witnessed substantial progress in both the theoretical and experimental understanding of such processes throughout the past decade. QCD predicts the partonic cross sections[1] for hard scattering at large momenta transfers. The determination of the production amplitudes for various final states requires the convolution of accurately determined parton distribution functions (PDF's)[2] with the partonic level cross sections to model the initial state parton momenta within the hadron beams. Pictorially jet production in hadron collisions can be modeled as in Fig. 1. Matrix elements for the hard interaction are available to (N)NLO/(N)NLL for many processes and phenomenological models tuned to data can be used to account for hadronization effects.

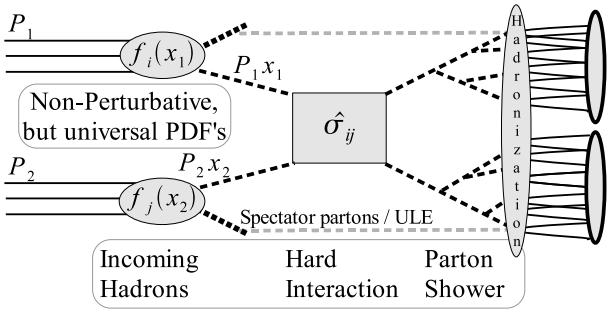

Figure 1. Jet production in hadron collisions. Matrix elements for the hard scatter are available at (N)NLO/(N)NLL for many processes under study. Non-perturbative parton distribution functions are factorized from the hard scattering cross section in calculating production rates at colliders.

This paper reviews the status of recent QCD studies from collider experiments at the Tevatron, HERA, and LEP.

2. Jet Production at the Tevatron

The available center-of-mass (cms) energy of $\sqrt{s} =$ (1.8)1.96 TeV for $p\overline{p}$ collisions at the Tevatron allows the experimental probe of distance scales down to $\sim 10^{-17}$ cm in measures of inclusive single jet and di-jet cross sections. This section summarizes the status of QCD jet analyses for the CDF[3] and DØ[4] experiments. Figures 2 and 3 show the kinematic regions accessed in measurements[5] of jet production in Run I at the Tevatron.[a]

The Run I history of QCD studies at the Tevatron includes the observation of a prominent excess of high-p_T central jet production (as compared to NLO predictions and contemporary PDF's) initially observed by the CDF experiment[6] and contrasted by the DØ observation with good agreement in shape and normalization between the data and theory.[7] (Figure 2 shows NLO QCD predictions for the DØ cross sections calculated with JETRAD.[8]) Analyses of experimental uncertainties showed the two data sets to be consistent and analyses of constraints in global fits for PDF's found that uncertainties in the determination of large-x gluon distributions, underlying assumptions in PDF parameterizations, and scale choices, allowed a very wide range of large-x behavior.[9] The dominant effect is due to poor constraints on the gluons at large-x from the data available for global fits. Ensuing discussions of these is-

[a] Run I refers to the data taking periods ending in 1996 with cms energy $\sqrt{s} = 1.8$ TeV. Run II refers to the current data run starting in 2001 with cms energy $\sqrt{s} = 1.96$ TeV.

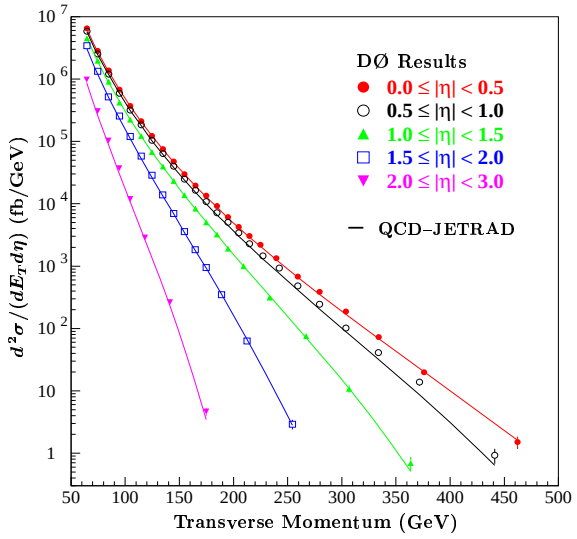

Figure 2. The single jet inclusive cross section measured in five bins of pseudorapidity from the DØ Run I data. Data are shown compared to NLO predictions for the cross sections.

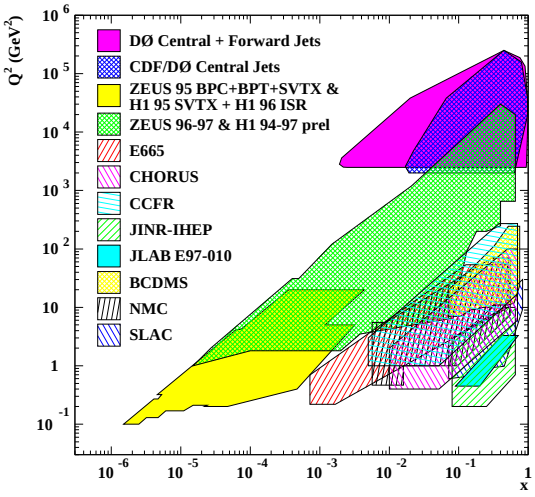

Figure 3. Kinematic reach of high-p_T jet data at the Tevatron compared to other colliders and fixed target experiments in the plane of parton momentum fraction x and square of the momentum transfer Q^2.

sues have directly contributed to an improved state-of-the-art in the reporting and applications of PDF uncertainties.[10]

In Run I both CDF and DØ performed most jet analyses using iterative cone algorithms based on the Snowmass standard.[11] Both experiments defined jets with cone radius $R = \sqrt{\Delta\eta^2 + \Delta\phi^2} = 0.7$. Where the polar (pseudorapidity, η^b) and azimuthal (ϕ) angles are defined by E_T weighted averages of all energy depositions associated with the jet.

Run II at the Tevatron brings numerous detector improvements to both DØ and CDF.[12,13] Additionally, the physics reach is extended with an increased center-of-mass energy of 1.96 TeV and an expected factor of 50 (minimum) increase in total integrated luminosity. An improved iterative cone algorithm based on 4-momenta clusters (as opposed to the E_T weighting schemes defined at Snowmass) has been proposed[14] to address IR divergences in the Run I schemes and to fully specify the treatment of overlapping cones. DØ has implemented this improved cone algorithm for all Run II cone-jet analyses. In the preliminary CDF analyses jets have been reconstructed using their legacy Run I algorithm.

CDF has presented results of their measure of the inclusive jet cross section in the central region defined by $0.1 < |\eta^{jet}| < 0.7$ for $177\,\mathrm{pb}^{-1}$ of accumulated Run II data. The effect of the increased Run II cms energy on CDF's central jet cross section is shown in Fig. 4(a). The observed increase in jet production cross section is in agreement with NLO predictions within experimental uncertainties. In Fig. 4(b) the data are compared to the NLO QCD calculation using the full set of CTEQ6.1[15] parameterizations of the parton density functions. The range of NLO predictions defined by the full set of parameterizations is contained in the envelope shown by the solid lines. The preliminary DØ central jet inclusive cross section shown in Fig. 5 is measured in the region $|\eta^{jet}| < 0.5$. Both experiments are in agreement with NLO predictions within experimental uncertainties. Due to the increased cms energy at the Tevatron the reach of this cross section measurement has already been extended by 150 GeV with respect to Run II (see Fig.4).

Successive recombination or k_T algorithms have been introduced to resolve problems of infrared singularities in parton jet clustering and to provide a theoretically "clean" procedure, free from ad-hoc or non-physical definitions. Both DØ[16] and CDF have repeated their central jet inclusive cross section measurement using the Ellis-Soper k_T algorithm[17] for jet reconstruction. The DØ data for the central ($|\eta^{jet}| < 0.5$) inclusive jet cross section for k_T jets are compared to the NLO QCD prediction and to

[b] $\eta = -ln(tan(\theta/2))$, where θ is the polar angle relative to the beamline.

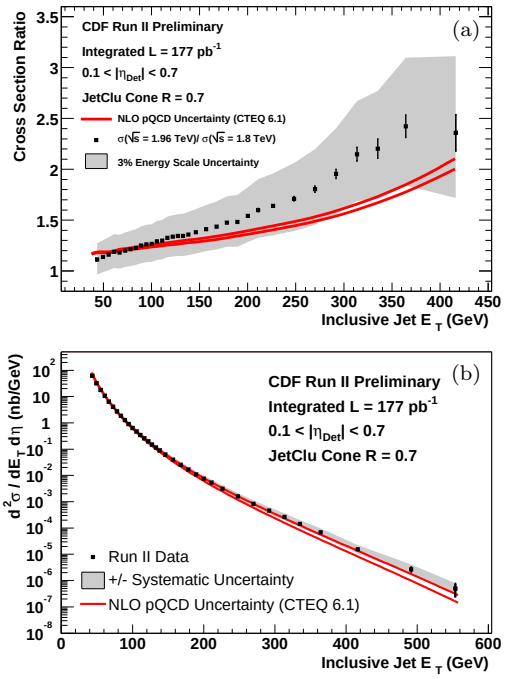

Figure 4. (a) Ratio of CDF's central inclusive jet cross section (Run II/Run I). (b) CDF's central inclusive jet cross section (circles) compared to NLO QCD (lines). The two lines represent limits on the ranges of predictions determined from the set of CTEQ6 parton density functions. Experimental systematic uncertainties are shown by the shaded band.

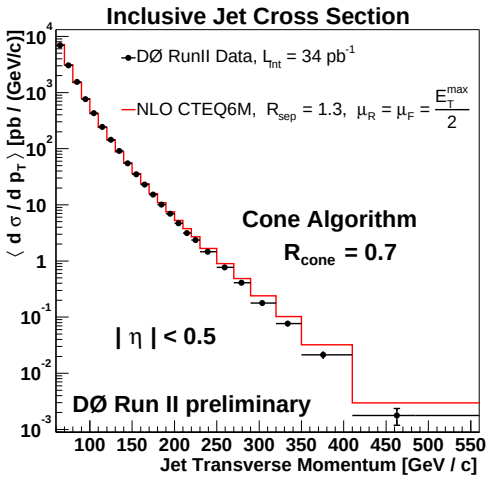

Figure 5. DØ's central inclusive jet cross section $d\sigma/dp_T$ as a function of p_T^{jet} integrated over $|\eta^{jet}| < 0.5$. Also shown is the NLO calculation using the CTEQ6M parton distributions.

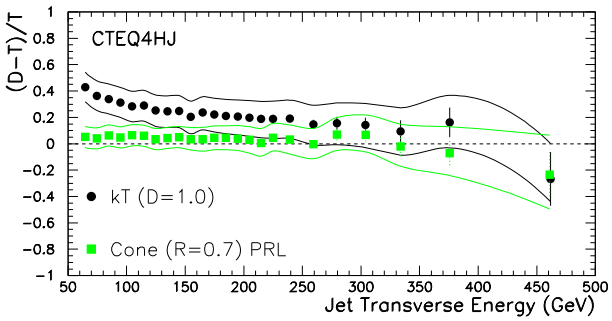

Figure 6. Fractional difference between DØ measurement of the inclusive jet cross section (D) compared to NLO QCD prediction (T) from Run I data. Jets reconstructed with k_T (circles) and cone (squares) algorithms are compared. Experimental systematic uncertainties (excluding luminosity) are shown by solid lines.

the cone jet cross section in the same η region in Fig. 6. The D-parameter used to control the size of the k_T jets was set to 1.0 for this analysis. The analysis used $88\,\mathrm{pb}^{-1}$ from the Run I data sample. Both DØ and CDF (not shown) find only marginal agreement with the NLO prediction at the lower p_T end of the spectrum. For the clustering algorithms in the DØ measurement, the NLO QCD predictions for the k_T and cone jet cross sections agree to within 1%. To identify the source of the difference between the data and theory, hadronization effects were evaluated using HERWIG to correct particle level jets back to the parton level. While k_T jets are found to appear more energetic at the hadron level as compared to cone jets, the magnitude of the difference was only found to be about one third of the observed difference in the data.

The di-jet mass cross section may also be used as a test of QCD, to constrain allowable PDF models, and to search for evidence of interactions beyond the Standard Model. The most strict limits on quark compositeness from Run I were obtained using di-jet measurements.[18] In di-jet analyses, reduction in experimental systematics due to detector resolution effects can compensate for reduced statistics due to the two jet requirement. Further, measuring the angular dependence of the jet production can reduce effects of PDF uncertainties when searching for new physics with relatively isotropic production angles. The preliminary DØ results for the di-jet mass cross section for Run II are summarized in Fig. 7. The data are in agreement with NLO QCD predictions within the experimental uncertainties. Preliminary results from CDF are shown in Fig. 8. A comparison with the Run I cross section is included to show the increased reach at Run II.

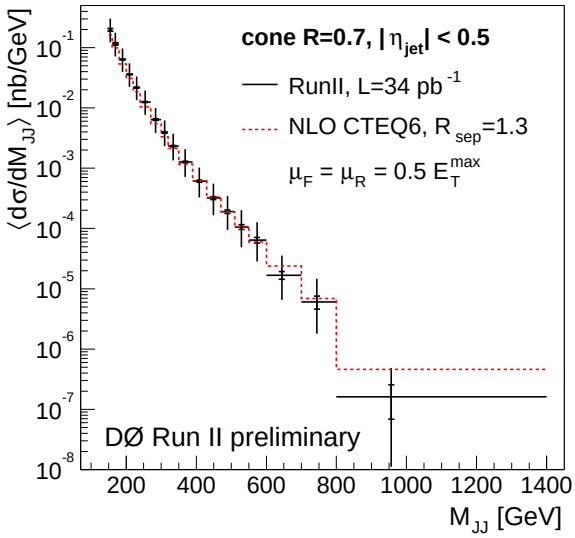

Figure 7. DØ dijet mass cross section. $d^3\sigma/dMd\eta_1 d\eta_2$ for $|\eta_{jet}| < 0.5$. Inner (outer) error bars show statistical (total) experimental uncertainties. The NLO calculation is shown by the dashed line.

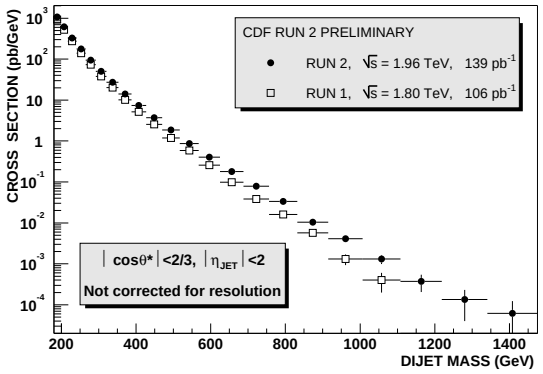

Figure 8. Di-jet mass cross section for CDF. The Run I data are overlaid to show the increased production rates in the Run II experiment.

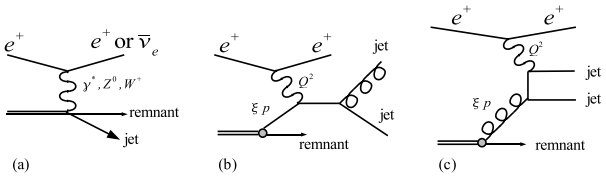

Figure 9. Order α_s diagrams for jet production in deep inelastic scattering. (a) Born, (b) QCD-Compton and (c) Boson-gluon fusion.

3. Jets in DIS and Photoproduction

This section summarizes recent experimental tests of QCD with jet production from the H1[19] and ZEUS[20] experiments at HERA. The HERA collider at DESY produces $e^{(+/-)}p$ collisions with a center-of-mass energy of 318 GeV. Precision measurements of the proton structure in ep deep-inelastic scattering (DIS) provide a strong verification of perturbative QCD, with a hard scale defined by Q^2, the virtuality of the photon exchange. Jet production gives direct access to the underlying parton dynamics and provides an additional scale, the jet transverse energy E_T, to describe the interaction within the framework of perturbative QCD. Figure 9 shows $O(\alpha_s)$ diagrams for jet production in ep DIS. Photoproduction will be discussed in Sec. 3.2.

3.1. *Jets in DIS*

Previous analyses of inclusive and multi-jet production in neutral current DIS at large virtualities[21] ($Q^2 > 125\,\mathrm{GeV}^2$) have shown excellent agreement with NLO QCD predictions. H1 has extended their measured inclusive jet cross sections to low Q^2 values in the range $5\,\mathrm{GeV}^2 < Q^2 < 100\,\mathrm{GeV}^2$. The low Q^2 analysis[22] shows the onset of discrepancies with NLO QCD predictions as demonstrated in Fig. 10. Jets are reconstructed using the inclusive k_T algorithm[17] and transverse energies are calculated in the Breit frame.[c] NLO calculations of jets observables were calculated using the DISENT program.[23] Corrections to the partonic cross section due to hadronization effects were estimated using a variety of Monte Carlo generators implementing the Lund color string model.[24]

Figure 10 shows the inclusive jet cross section versus jet E_T for three regions of pseudorapidity η_{lab}. Positive or forward η_{lab} is defined to be in the direction of the proton. Good agreement between the data and NLO QCD is observed in the backward region for all E_T's, while discrepancies become apparent in more forward regions, especially for jets with low E_T. The estimated renormalization scale uncertainties do not cover the discrepancies at lowest E_T in this region, where NLO corrections and scale sensitivity are also at their largest.

[c] In the Breit frame the photon and parton collide head-on ($2x\overline{p} + \overline{q} = 0$, where x is the Bjorken scaling variable, and $\overline{p}, \overline{q}$ are the proton and γ^* momentum, respectively). In this frame a jet produced at the Born level is defined to have $p_T = 0$.

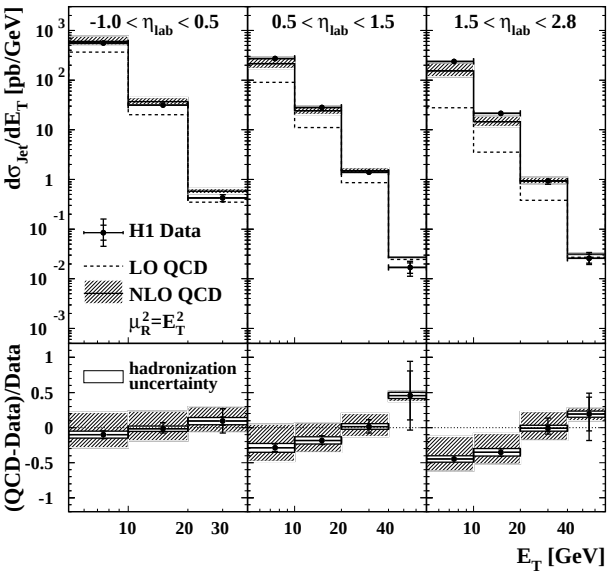

Figure 10. H1 measurements of inclusive jet cross sections $d\sigma/dE_T$ integrated over the region $5 < Q^2 < 100\,\mathrm{GeV}^2$. The data are shown as points. Error bars include statistical and systematic uncertainties. Top frame: Data are compared to DISENT NLO QCD calculations using CTEQ5M PDF's (solid line) and DISENT LO calculations using CTEQ5L (dashed line), with renormalization scale $\mu_R = E_T$ (no hadronization corrections are applied). The effects of varying μ_R by factors of ± 2 are shown in the hatched band. Bottom frame: (QCD-Data)/Data, where "QCD" denotes NLO QCD corrected for hadronization effects. Hadronization uncertainties are denoted by the inner white band.

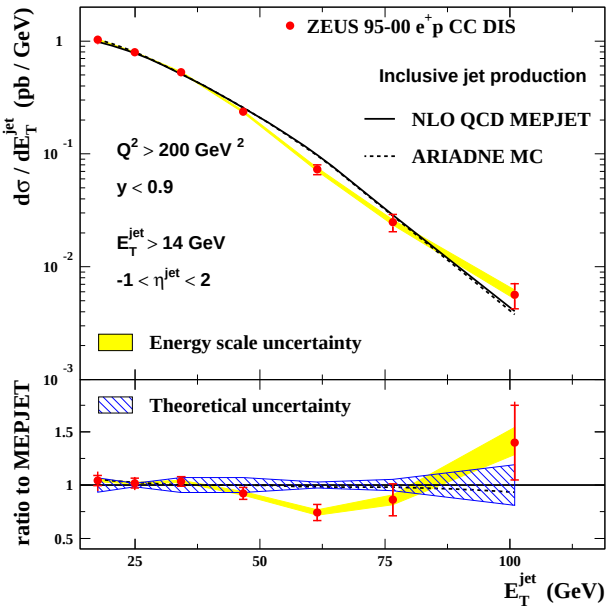

Figure 11. (a) Differential cross section, $d\sigma/dE_T$ for inclusive jet production measured at ZEUS (dots) with $E_T^{jet} > 14\,\mathrm{GeV}$ and $-1 < \eta^{jet} < 2$ with $Q^2 > 200\,\mathrm{GeV}^2$. The solid band shows the uncertainty due to the calorimeter energy scale. Error bars are statistical (inner) and statistical $\oplus$ systematic (outer), exclusive of the scale error. (b) Ratio of the measured cross section to NLO calculation. The hatched band represents the theoretical uncertainty.

The ZEUS experiment has measured inclusive and di-jet production rates[25] and jet substructures in charged current (CC) DIS for $Q^2 > 200\,\mathrm{GeV}^2$. Jet production in CC DIS provides a testing ground for both QCD and the electroweak sector of the Standard Model. Up to leading-order in α_s CC DIS proceeds via the QCD-Compton ($Wq \to q'g$), W-gluon-fusion ($Wg \to q\overline{q}'$), or the pure electroweak process ($Wq \to q'$). The inclusive jet cross section for $E_T^{jet} > 14\,\mathrm{GeV}$ and $-1 < \eta^{jet} < 2$ is shown in Fig. 11. The data sample corresponds to an integrated luminosity of $110.5\,\mathrm{pb}^{-1}$. Jets were reconstructed using the invariant k_T algorithm in the laboratory frame. Both the NLO QCD calculation of MEPJET[26] and the LO ARIADNE MC[27] models give a good description of the jet cross section. The NLO calculations were corrected to the hadron level using ARIADNE and LEPTO[28] models to estimate the uncertainty on the procedure.

It is interesting to contrast the agreement of the HERA cross sections and NLO QCD for low E_T jets defined using the k_T algorithm with the Tevatron k_T jet measurements. Correction for hadronization effects at the Tevatron does not recover good agreement at lower E_T values. This may suggest complications due to more energetic underlying events in the $p\bar{p}$ collisions at the Tevatron.

3.2. *Jets in Photoproduction*

A comparison of measurements of jet production at different center-of-mass energies demonstrates scaling violations due to the evolution of structure functions and the running of the strong coupling constant α_s. In the parton model the scaled jet invariant cross section, $S(x_T) = (E_T^{jet})^4 E^{jet} d^3\sigma/dp_X^{jet} dp_Y^{jet} dp_Z^{jet}$, should be independent of W, the center-of-mass energy, when plotted against the dimensionless variable $x_T = 2E_T^{jet}/W$. Scaling violations have been observed in $p\bar{p}$ collisions at center-of-mass energies of 546(630) and 1800 GeV.[29] Photoproduction of jets in ep collisions can be used to perform similar tests. Photoproduction is differentiated from neutral current DIS, by requiring a small virtuality of the ex-

changed photon, typically $Q^2 < 1\,\mathrm{GeV}^2$. Hence the photons are quasi-real and γp collisions may be studied. The photon may act as a point-like particle in an interaction with a parton carrying a fraction x_p of the proton momentum (direct process). Alternatively the photon may develop a hadronic structure (resolved process) where a parton carrying a fraction x_γ of the photon momentum interacts with a parton in the proton.

ZEUS has measured the scaled jet invariant cross section[30] in γp collisions for the γp center-of-mass energy range $142 < W_{\gamma p} < 293\,\mathrm{GeV}$ for the pseudorapidity range $-2 < \eta^{jet} < 0$. Event selection requires $Q^2 < 1\,\mathrm{GeV}^2$, yielding a median $Q^2 \sim 10^{-3}\,\mathrm{GeV}^2$. The data are divided into two center-of-mass ranges with $\langle W_{\gamma p}\rangle = 180$ and $255\,\mathrm{GeV}$. Figure 12 shows the ratio of the scaled invariant cross sections as a function of x_T. The clear deviation from unity is in agreement with NLO QCD predictions, which include the running of α_s and evolution of PDF's with the scale. These data constitute the first observation of scaling violations in γp collisions. The cross section $d\sigma/dE_T^{jet}$ as a function of E_T^{jet} was used to determine $\alpha_s(M_Z)$.[30] The value $\alpha_s(M_Z)$ was obtained in each bin of the measured cross section and from χ^2 fits to all the data: $\alpha_s(M_Z) = 0.1224 \pm 0.0001(\mathrm{stat.})^{+0.0022}_{-0.0019}(\mathrm{exp.})^{+0.0054}_{-0.0042}(\mathrm{th.})$. NLO calculations with hadronization corrections are used throughout the analysis. The largest contribution to the experimental uncertainty ($\pm 1.5\%$) arises from the jet energy scale. The largest contribution to the theoretical uncertainty arises from terms beyond NLO ($^{+4.2}_{-3.3}\%$). For a full discussion see the References.[31]

H1 has also reported a new measurement of inclusive jet production in photoproduction[32] based on $24.1\,\mathrm{pb}^{-1}$ of e^+p data. Jets were reconstructed using the k_T algorithm for $-1 < \eta^{jet} < 2.5$ in the laboratory frame. Events were selected with $Q^2 < 1\,\mathrm{GeV}^2$ and $E_T^{jet} \geq 21\,\mathrm{GeV}$. The γp cms energy range for these events was $95 \leq W_{\gamma p} \leq 285\,\mathrm{GeV}$. The measurement was extended down to $E_T^{jet} \geq 5\,\mathrm{GeV}$ using a $0.47\,\mathrm{pb}^{-1}$ collected via a dedicated trigger. The kinematic range for these data is $Q^2 \leq 0.01\,\mathrm{GeV}^2$ and $164 \leq W_{\gamma p} \leq 242\,\mathrm{GeV}$. Figure 13 shows a measurement of the inclusive jet cross section over the entire E_T range after combining the two samples. The samples were combined by applying a common $W_{\gamma p}$ cut ($164 \leq W_{\gamma p} \leq 242\,\mathrm{GeV}$) and by correcting

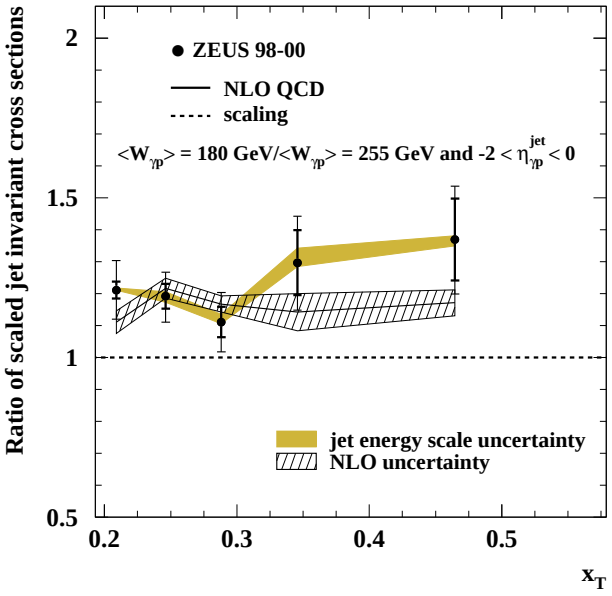

Figure 12. Ratio of scaled jet invariant cross sections versus x_T for two intervals ($W_{\gamma p}$) of γp center-of-mass energies in photoproduction measured at ZEUS.

the low E_T sample by the difference in photon flux $f_{\gamma/e}(y, Q^2)$ over ranges $Q^2 < Q^2_{max}$ for the two samples. The fraction of the electron energy carried by the photon is given by $y = E_\gamma/E_e$. The measured cross section $d\sigma/dE_T^{jet}$ falls by more than 6 orders of magnitude and is well produced by the theoretical prediction. Hadronization corrections are needed in addition to NLO contributions for good agreement with the data at low E_T^{jet}.

The photoproduction results are compared with measurements in $p\overline{p}$ collisions to observe differences arising from the structures of the photon and the proton. The differential cross section was redetermined using a cone algorithm with radius $R = 1$ to match the procedure used for available $p\overline{p}$ data at a comparable cms $\sqrt{s} = 200\,\mathrm{GeV}$.[33] To compare with $p\overline{p}$ measurements at different energies, the cross section was measured with the cone algorithm in the restricted range $1.5 \leq \eta^{jet} \leq 2.5$ and for $E_T^{jet} > 8\,GeV$ and scaled to the invariant cross section at fixed $W_{\gamma p} = 200\,\mathrm{GeV}$ averaged over the cms pseudorapidity range $|\eta^*| \leq 0.5$ using Monte Carlo models to evaluate the correction factors. The invariant scaled cross section is compared to data from UA2[33] and DØ[5,34] in Fig. 14. The $p\overline{p}$ data were transformed into $S(x_T)$ using the central bin values and were scaled by factors of $O(\alpha_{em}/\alpha_s)$ to match the photoproduction

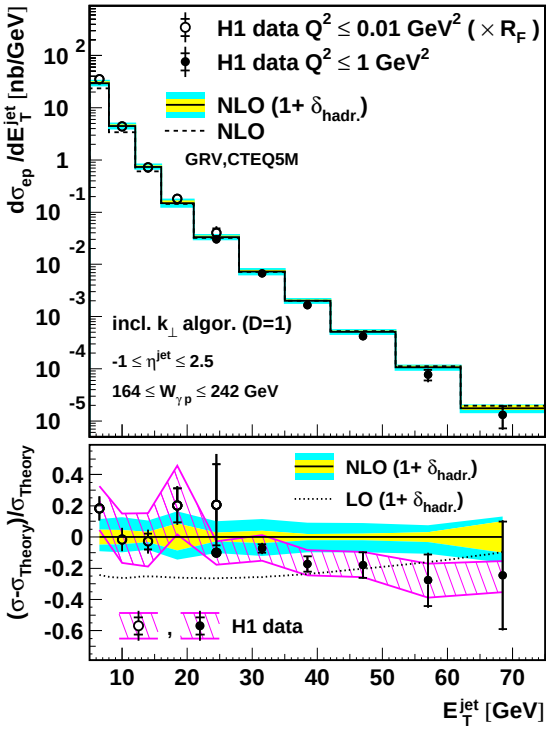

Figure 13. H1 inclusive jet photoproduction. Top: the differential e^+p cross section $d\sigma/dE_t^{jet}$ for inclusive jet production integrated over $-1 \leq \eta^{jet} \leq 2.5$ and $Q^2 \leq 1\,\mathrm{GeV}^2$ (filled circles). Low E_T data measured for $Q^2 \leq 0.01\,\mathrm{GeV}^2$ shown by open circles are corrected for the ratio of photon fluxes in the two Q^2 regions. Bottom: fractional difference between the data (or LO QCD prediction) and the NLO calculation with hadronization corrections. The PDF's used for the photon and proton were GRV and CTEQ5M, respectively.

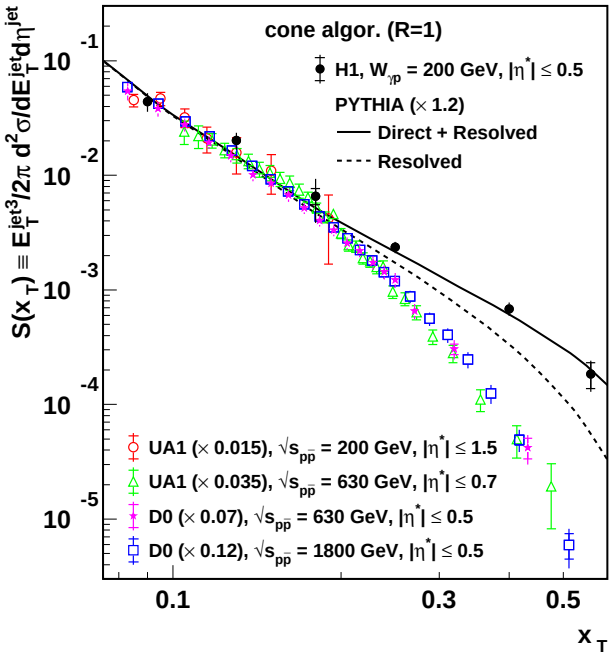

Figure 14. H1 inclusive jet photoproduction. The scaled γp cross section at $W_{\gamma p} = 200\,\mathrm{GeV}$ for inclusive jet production as a function of x_T for $|\eta^*| < 0.5$. Jets are found with a cone algorithm ($R = 1$) and the data are compared with measurements from UA2 and DØ of the inclusive jet cross section at various cms energies. Predictions of PYTHIA for the direct γp and resolved photon contributions are also shown (a normalization factor of 1.2 is applied).

data at $x_T \sim 0.1$. Despite differences in η intervals and analysis procedures, all $p\overline{p}$ data are in approximate agreement. The γp data are compatible with the $p\overline{p}$ data in the region $x_T \lesssim 0.2$, where the resolved photon leads to scaling behavior similar to that for a hadron. At larger x_T the shape of the γp cross section deviates from the $p\overline{p}$ measurements. This is a result of the enhanced quark density of the resolved photon relative to that of the proton at large momentum fractions. Dominating the scaled cross section at largest x_T, the direct photon contribution involves the convolution of only the proton PDF's.

4. $\gamma\gamma$ Collisions at LEP

High energy hadrons at LEP are mainly produced via the process $e^+e^- \to e^+e^-\gamma^*\gamma^* \to e^+e^- + hadrons$, where hadrons of large transverse momentum are produced directly from the virtual photons (QED process $\gamma^*\gamma^* \to q\overline{q}$) or via QCD processes if the partonic content of the photons is resolved. L3 has measured the differential cross sections $d\sigma/dp_T$ for the production of high-p_T hadrons and jets in two-photon collisions. Distributions for charged pions and jets are shown in Fig. 15. Events were selected based on low photon virtuality $\langle Q^2 \rangle \simeq 0.2\,\mathrm{GeV}$ and an effective mass of the $\gamma\gamma$ system $W_{\gamma\gamma} \geq 5\,\mathrm{GeV}$. The published results for charged pion production[35] show a clear excess of events as compared to NLO QCD for $p_T > 5\,\mathrm{GeV}$. A recent analysis performed for jets confirms the observation of excess production at high p_T. Both analyses were restricted to the region $|\eta| < 1.0$ and jets were reconstructed using the k_T algorithm[17] with a minimum p_T requirement of 3 GeV with a D-cut of 1.0.

In Fig. 15(b) the jet data are compared to NLO analytical QCD predictions.[36] The flux of quasi-real photons was obtained via the Weizsäcker-Williams formula.[37] Both the direct and resolved production processes were included in the NLO calcula-

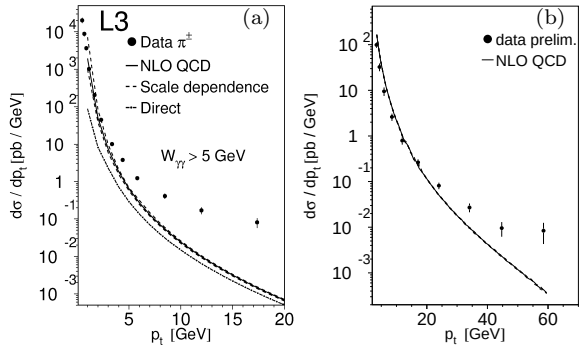

Figure 15. L3 measurements of inclusive differential cross sections $d\sigma/dp_T$ in $\gamma\gamma$ collisions for charged pion production (a) and jet production (b). The data (preliminary) are compared to NLO calculations (solid lines). Scale uncertainties are shown in dashed lines. The dashed-dot line corresponds to the direct process ((a) only).

tion. Parton densities were modeled using GRV-HO.[38] Scale uncertainties calculated by varying the scale up/downward by a factor of two are small. Poor agreement is observed in the high-p_T jet region as in other channels. The cause of this excess has yet to be explained.

The OPAL experiment has measured the production of di-jets at center-of-mass energies $\sqrt{s_{ee}}$ from 189-209 GeV. Jets were reconstructed using the k_T algorithm and the event selection required at least 2 jets with $|\eta^{jet}| < 2$, $E_T^{jet} > 3\,\mathrm{GeV}$. A cut of $Q^2 < 4.5\,\mathrm{GeV}^2$ was used to select quasi-real photons. Backgrounds from hadronic decays of the Z^0, $\gamma\gamma \to \tau\tau$, and $\gamma\gamma^*$ collisions were subtracted. For single or double resolved processes the variables $x_\gamma^\pm$ estimate the fraction of the photon's momentum participating in the hard scattering. At LO all of the photon's energy goes into the two jet final state ($x_\gamma^\pm = 1$). Whereas for single and double resolved events one or both x_γ values will be less than 1, with:

$$x_\gamma^\pm = \frac{\sum_{jet_{1,2}} E \pm p_z}{\sum_{hadrons} E \pm p_z}. \qquad (1)$$

The data are compared to LO and NLO QCD predictions[39] in Fig. 16. The cross section is plotted versus the mean jet transverse energy $\langle E_T^{1,2} \rangle$. At large $\langle E_T^{1,2} \rangle$ the cross section is expected to be dominated by direct processes, consequently a softer spectrum is observed in single (double) resolved enhanced subsamples. The NLO calculation using GRV-HO parton densities is in good agreement with the full data sample and for single resolved enhanced events (x_γ^+ or $x_\gamma^- < 0.75$). Predictions for a double resolved enhanced sample (x_γ^+ and $x_\gamma^- < 0.75$) are below the measurement. Good agreement is found with PYTHIA and SaS 1D[40] parton densities. Observables in the double resolved region may be used to study effects of multiple parton interactions in greater detail.

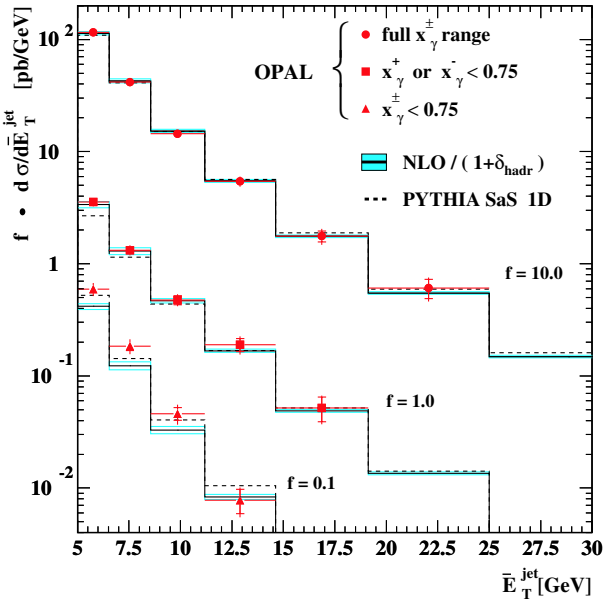

Figure 16. Di-jet cross section versus mean jet transverse energy $\langle E_T^{1,2} \rangle$ for three regions of x_γ. Distributions are shown for the full sample, single resolved enhanced (x_γ^+ or $x_\gamma^- < 0.75$), and double resolved enhanced subsamples (x_γ^+ and $x_\gamma^- < 0.75$). The data are compared to PYTHIA using SaS 1D parton densities and a NLO perturbative prediction using GRV-HO densities.

5. Event Shapes and α_s

Distributions of event shape variables are predicted to various orders in pQCD. Fits to measurements of these distributions may be used to determine the value of the strong coupling constant. Studies at LEP and HERA have used this technique to extract measurements of α_s.

Preliminary results from the LEP QCD Working Group[41] were presented at the conference. The Working Group is charged with combining the various event shape analyses from the four LEP experiments to obtain the best statistical precision for this measurement of α_s. Combining four equally weighted experiments would naïvely reduce statisti-

cal uncertainties by a factor of two and combining different events shape measurements would reduce the uncertainty further. However, different event shape variables within a single experiment will not be statistically independent in general, and consistent treatments of systematic uncertainties must be applied to combine results across experiments. The LEP event shape analysis combines a total of 194 measurements spanning 4 experiments, 15 cms energies, and 6 shape variables.

The event shape variables studied include:

Thrust, $T = \left(\frac{\sum_i |\vec{p_i}\cdot\vec{n}|}{\sum_i |\vec{p_i}|}\right)$: $\vec{n}$ is chosen to be the thrust axis $\vec{n_T}$ such that the quantity T is maximized.

Heavy Jet Mass, $M_H/\sqrt{s}$: Using a plane through the origin and perpendicular to $\vec{n_T}$ the event is split into two hemispheres and invariant masses are calculated using the particles in each hemisphere. M_H is the larger of the two mass values.

Jet Broadening, B_T and B_W: Measure the broadening of particles in transverse momentum w.r.t. the thrust axis for all particles and those in the hemisphere with the most broadening respectively.

C-parameter, C: Based on eigenvalues of the momentum tensor of the event.[42]

Two-to-3 jet transition parameter, y_3: Based on y_{cut}, the jet resolution parameter in the Durham scheme for combining particles into jet clusters. y_3 is defined as the maximum value of y_{cut} that produces three separate jets.

Each experiment provided results for the observables: thrust, heavy jet mass, C-parameter, wide and total jet broadening. ALEPH and OPAL provided measurements of $-log(y_3)$. Most measurements were performed for cms energies between 91 and 206 GeV. L3 additionally performed measurements between 41 and 85 GeV using radiative events at the Z^0 peak.

Experimental uncertainties are averaged over all experiments for each variable to prevent bias in favor of experiments with the least conservative error estimates. Monte Carlo generators are used to account for non-perturbative effects due to hadronization effects. Hadronization uncertainties are estimated based on the differences among the three generators PYTHIA, HERWIG, and ARIADNE. Theoretical uncertainties are estimated by measuring the scale dependence of the fits. Details may be found in the References.[43] The combination procedure takes correlations between the measurements into account. A 194×194 covariance matrix V is defined relating the uncertainties for all pairs of $\alpha_s(M_Z^0)$ measurements. The covariance matrix is expressed as the sum of four sources of error:

$$V_{ij}^{total} = V_{ij}^{stat} + V_{ij}^{exp} + V_{ij}^{hadr} + V_{ij}^{theo}. \quad (2)$$

Then the method of least-squares is used to calculate the maximum-likelihood value of $\alpha_s(M_Z^0)$. Figure 17 shows the combined value of $\alpha_s(M_Z^0)$ and individual values broken down as a function of the six event shape variables. The preliminary result for the combined measurements is: $\alpha_s(M_Z^0) = 0.1201 \pm 0.0003(\text{stat.}) \pm 0.0048(\text{syst.})$.

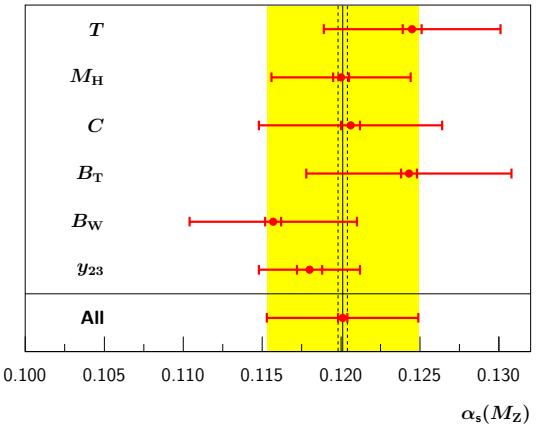

Figure 17. LEP combined $\alpha_s(M_Z^0)$ from event shape analyses (preliminary) broken down as a function of each event shape variable. The inner error bars and dashed band represent statistical errors. The shaded band and outer error bars represent the total uncertainty in the measurement.

Figure 18 shows a summary of $\alpha_s(M_Z^0)$ results from hadronic processes with the new LEP measurement included. While the most precise measurements of $\alpha_s(M_Z)$ come from $\Gamma(Z \to \tau\tau)$ and τ decays, the hadronic processes offer a strong verification of the Standard Model and in many cases their ultimate precision is limited only by the availability of higher order theoretical corrections.

Analyses have also been performed at LEP[44] and HERA[45,46] to extract $\alpha_s(M_Z^0)$ from event shapes by modeling non-perturbative effects via QCD inspired power corrections. The non-perturbative effects in event shape variables are taken to scale with powers

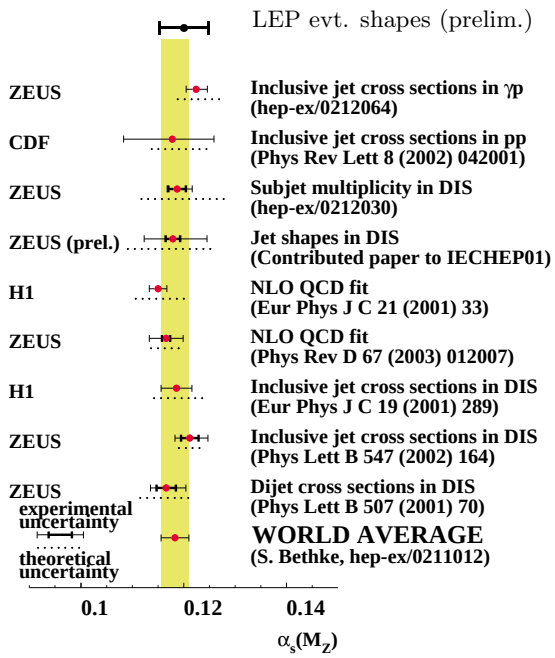

Figure 18. Summary of measurements of $\alpha_s(M_Z^0)$ from hadronic processes. Inner (outer) error bars represent statistical (statistical+systematic) errors. Dotted lines show theoretical uncertainties. All uncertainties are combined in the LEP point.

of $1/Q$ and the model of Dokshitzer and Webber[47] is used to parameterize the infrared behavior of the strong coupling by its mean value below a matching scale μ_I. A recent fit[45] from H1 using power law corrections to event shape distributions is shown in Fig. 19. The event shape variables follow similar definitions to the LEP analyses, for details see the References.[45] This result verifies the universality of power law corrections for event shape distributions.

6. Heavy Flavor Production

Figure 20 shows a preliminary measurement of the inclusive b-jet inclusive cross section measured at DØ using $3.4\,\mathrm{pb}^{-1}$ of integrated luminosity from the Run II data. Events were selected with $|\eta^{jet}| < 0.6$, $E_T^{jet} > 20\,\mathrm{GeV}$ and at least one muon satisfying $|\eta^{\mu}| < 0.8$ and $E_T^{\mu} > 6\,\mathrm{GeV}$. Backgrounds to muons from b decays were subtracted by fitting[48] the p_T^{rel} distribution[d] in each bin with signal and background components of the total p_T^{rel} calculated with PYTHIA. The Run II measurement is compared to PYTHIA, and as observed previously,[48] the cross section is ∼2 times larger than predictions.

[d] p_T of muon measured relative to jet axis.

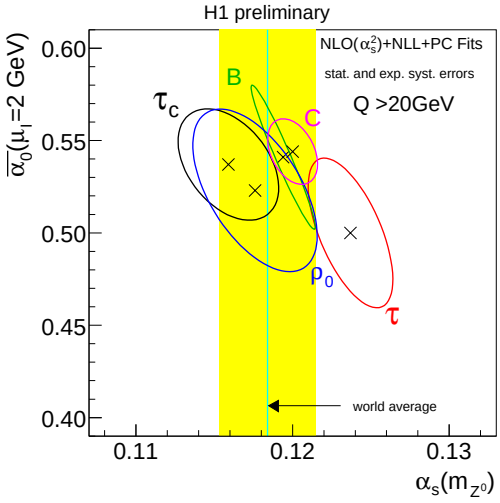

Figure 19. Mean values and 1σ contours of $\alpha_s(M_Z)$ and $\overline{\alpha}_0$ fitted to distributions of event shape variables from H1. $\overline{\alpha}_0$ is the effective value of the strong coupling constant below the cut-off scale μ_I.

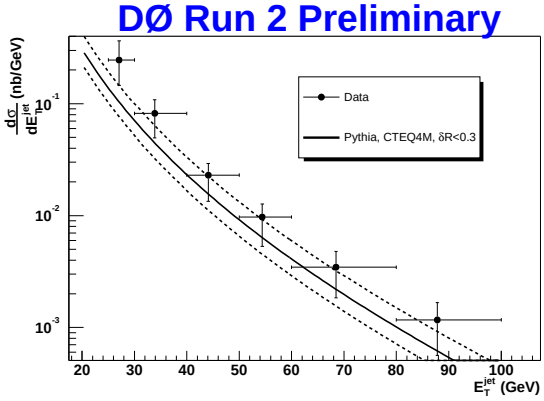

Figure 20. DØ preliminary measurement of b production cross section compared to a PYTHIA+CTEQ4M calculation. Only the LO prediction is shown. Scale uncertainties are represented by the dashed lines.

CDF has shown a preliminary measure of charm production in the cross sections for the D^0, D^+ and D^{*+}. A measure of the cross section $d\sigma/dp_T(D^0)$ for D^0 production versus transverse energy is shown in Fig. 21. The data are observed to lie above the NLO calculations[49] by a factor of ∼1.7.

Both H1 and ZEUS have measured beauty production[50] in photoproduction and DIS events. Preliminary results for beauty in photoproduction for the process $ep \to eb\bar{b}X \to ejj\mu X$ is shown in Fig. 22. All data points lie above the NLO QCD prediction, but are in agreement within experimental errors.

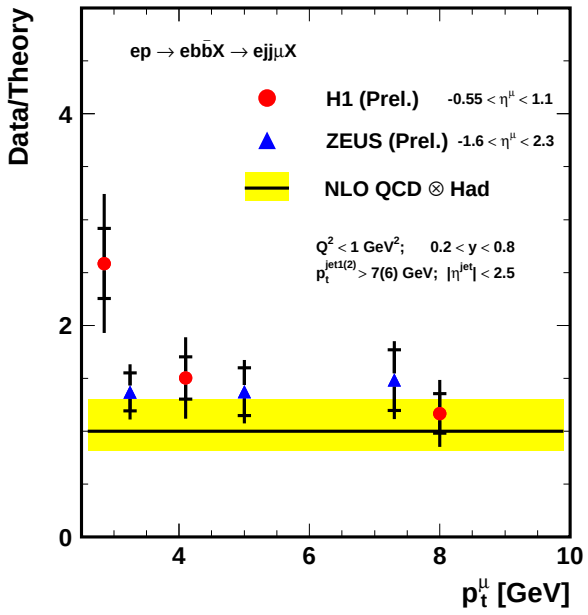

Figure 22. Ratio of the differential di-jet muon beauty cross section $d\sigma/dp_T^\mu$ ($ep \to eb\bar{b}X \to ejj\mu X$) from H1 ($-0.55 < \eta^\mu < 1.1$) and ZEUS ($-1.6 < \eta^\mu < 2.3$) to NLO QCD with hadronization corrections. The shaded band shows the uncertainty in the calculation due to scale variations.

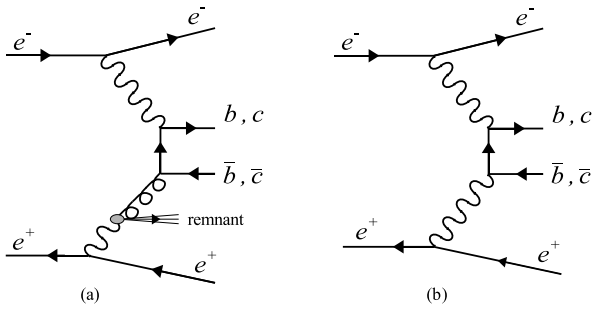

Figure 23. Production of open charm and beauty at LEP2 in two photon collisions proceeds primarily through either the single resolved (a) or direct (b) processes shown above.

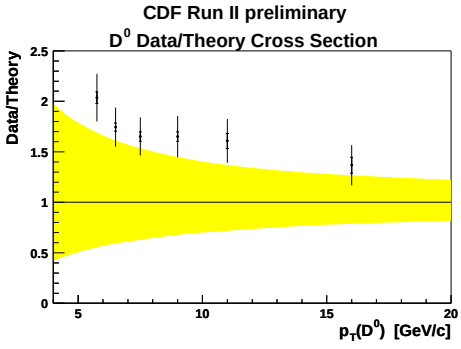

Figure 21. The CDF ratio of cross section for D^0 production to NLO QCD prediction $d\sigma/dp_T(D^0)$.

Open charm and beauty production have been studied at LEP in two photon collisions. The two main contributions to the cross sections $\sigma(e^+e^- \to e^+e^-c\bar{c}X)$ and $\sigma(e^+e^- \to e^+e^-b\bar{b}X)$ are the direct and single resolved processes illustrated in Fig. 23. Figure 24 shows the LEP measurements of open charm and beauty compared with the NLO QCD predictions.[51] The charm rate agrees well with the data, but requires the inclusion of the single resolved process for agreement. Beauty production rates are about a factor of two larger than predictions.

7. Summary

We continue to see tremendous progress in the experimental study of QCD at the world's colliders. The theory survives admirably, though increasingly precise data highlight the need for further progress in the theoretical calculations, particularly the need for higher order corrections to confront increasingly precise jet data. It will be interesting to see if other advances, perhaps in resummation techniques, can explain the trends toward higher cross sections for heavy flavor production. On the experimental side, work clearly remains on understanding k_T jets at the hadron colliders.

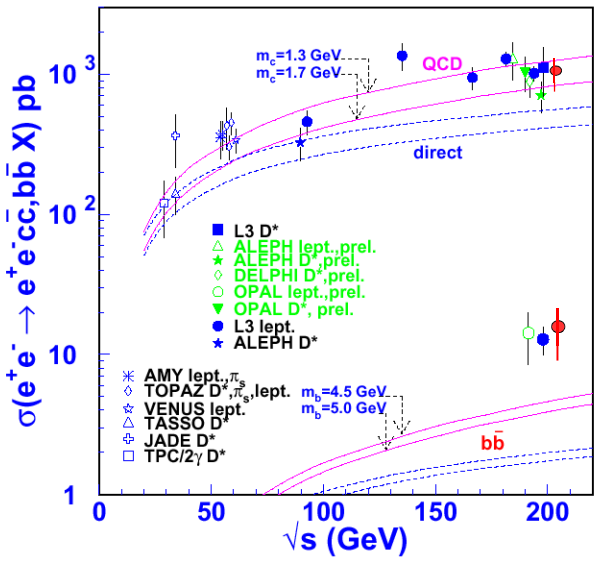

Figure 24. Cross sections for production of open charm and beauty at LEP2

Acknowledgments

I wish to thank the numerous physics conveners and collaborators from ALPEH, DELPHI, L3, OPAL, H1, ZEUS, CDF and DØ for their help in preparing this talk.

References

1. F. Aversa et al., *Phys. Rev. Lett* **65**, 401 (1990); W. T. Giele, E. W. N. Glover, and D. A. Kosower, *Phys. Rev. Lett* **73**, 2019 (1994); D. Ellis, Z. Kunszt, and D. E. Soper, *Phys. Rev. Lett* **64**, 2121 (1990).
2. P. Newman, these proceedings.
3. F. Abe, *Nucl. Instru. Meth* A **271**, 387 (1988).
4. S. Abachi *et al.*, *Nucl. Instru. Meth* A **338**, 185 (1994).
5. B. Abbott *et al.*, *Phys. Rev. Lett.* **86**, 1707 (2001).
6. F. Abe *et al.*,*Phys. Rev. Lett* **77**, 438 (1996).
7. B. Abbott *et al.*, *Phys. Rev. Lett.* **82**, 2451 (1999).
8. W. T. Giele, E. W. N. Glover, and D. A. Kosower, *Nucl. Phys.* B **403**, 633 (1993); *Phys. Rev. Lett* **73**, 2019 (1994).
9. S. Kuhlmann, H. L. Lai, W. K. Tung, *Phys. Lett.* B **409**, 271 (1997).
10. R. Thorne these proceedings.
11. J. E. Huth, *et al.*, in Proceedings of Research Directions for the Decade: Snowmass 1990, July 1990, edited by E. L. Berger (World Scientific, Singapore, 1992) p. 134.
12. P. Petroff, hep-ex/9910028.
13. M. Paulini, FERMILAB-CONF-03/010-E.
14. G. C. Blazey *et al.*, Run II jet physics, hep-ex/0005012, 2000.
15. D. Stump *et al.*, hep-ph/0303013.
16. V. M. Abazov *et al.*, *Phys. Lett.* B **525**, 211 (2002).
17. S. D. Ellis, D. E. Soper, *Phys. Rev.* D **48**, 3160 (1993); S. Catani *et al.*, *Nucl. Phys.* B **406**, 187 (1993).
18. B. Abbott *et al.*, *Phys. Rev. Lett.* **82**, 2457 (1999); *Phys. Rev.* D **64**, 032003 (2001).
19. I. Abt *et al.*, *Nucl. Instru. Meth* A **386**, 310 (1997); I. Abt *et al.*, *Nucl. Instru. Meth* A **386**, 348 (1997).
20. ZEUS Collaboration, U. Holm (ed.), *The ZEUS Detector* Status Report (unpublished), DESY (1993), http://www-zeus.desy.de/bluebook/bluebook.html.
21. *Eur. Phys. J.* C **19**, 289 (2001); *Phys. Lett.* B **515**, 17 (2001); *Eur. Phys. J.* C **23**, 13 (2002); *Phys. Lett.* B **507**, 70 (2001).
22. H1 Collaboration, DESY-02-079.
23. S. Catani and M. H. Seymore, *Nucl. Phys* B **485**, 45 (1999).
24. B. Andersson *et al.*, *Phys. Rept.* **97**, 31 (1983).
25. DESY-03-055, June 2003.
26. E. Mirkes and D. Zepenfeld, *Phys. Lett.* B **380**, 205 (1996).
27. L. Lönnbald, *Comp. Phys. Comm* **71**, 15 (1992); L. Lönnbald, *Z. Phys.* C **65**, 285 (1995).
28. G. Ingleman, A. Edin and J. Rathsman, *Comp. Phys. Comm* **101**, 108 (97).
29. F. Abe *et al.*, *Phys. Rev. Lett* **70**, 1376 (1993); B. Abbott *et al.*, *Phys. Rev. Lett* **86**, 2523 (2001).
30. J. Breitweg *et al.*, *Phys. Lett.* B **507**, 70 (2001); S. Chekanov *et al.*, *Phys. Lett.* B **547**, 164 (2002).
31. DESY-02-228, December 2002.
32. H1 Collaboration DESY-02-225.
33. C. Albajar *et al.*, *Nucl. Phys.* B **309**, 405 (1988); G. Arinson *et al.*; *Phys. Lett.* B **172**, 461 (1986).
34. B. Abbott *et al.*, *Phys. Rev. Lett.* **82**, 2451 (1999).
35. The L3 Collaboration, *Phys. Lett.* B **554**, 105 (2003).
36. S. Frixione, *Nucl. Physics* B **507**, 295 (1997); S. Frixione and G. Ridolfi, *Nucl. Physics* B **507**, 315 (1997).
37. C. F. von Weizsäcker, *Z Phys.* **88**, 612 (1934); E. J. Williams, *Phys. Rev.* **45**, 729 (1934).
38. M. Gluck, E. Reya and A. Vogt, *Phys. Rev.* D **45**, 3986 (1992); M. Gluck, E. Reya and A. Vogt, *Phys. Rev.* D **46**, 1973 (1992).
39. M. Klasen, T. Kleinwort, G. Kramer *Euro. Phys. J Direct* **C1**, 1 (1998); B. Pötter *Euro. Phys. J Direct* C **5**, 1 (1998).
40. G. A. Schuler and T. Sjöstrand *Z. Phys.* C **68**, 607 (1995).
41. The LEP QCD Working Group: S. Banerjee, M. Ford, R. Jones, G. Salam, H. Stenzel and D. Wicke; contact Roger.Jones@cern.ch.
42. G. Parisi, *Phys. Lett.* B **74**, 65 (1978); J. F. Donoghue, F. E. Low and S. Y. Pi, *Phys. Rev.* D **20**, 2759 (1979).
43. R. W. L. Jones, M. Ford, G. P. Salam, H. Stenzel, in preparation.
44. DELPHI 2003-019 CONF 639, June 2003.
45. H1 Note H1prelim-03-033.
46. ZEUS Collaboration, DESY-02-198.
47. Y. L. Dokshitzer and B. R. Webber, *Phys. Lett.* B **404**, 321 (1997).
48. B. Abbott *et al.*, *Phys. Rev. Lett.* **85**, 5068 (2000).
49. P. Nason and M. Cacciari, hep-ph/0306212.
50. See list of contributed papers to this conference.
51. Drees, Kramer, Zunft and Zerwas, *Phys. Lett.* B **306**, (1993).

DISCUSSION

Lance Dixon (SLAC): I think you only showed us Tevatron jet data using the Run I algorithm. Are there Run II data using improved jet algorithms, say, infrared-safe algorithms?

Robert Hirosky: Yes, in my discussion of the DØ data, I mentioned that jets are reconstructed using the Run II mid-point algorithm. That is an infrared-safe algorithm.

Doris Kim (University of Illinois): You mentioned that the charm and beauty cross section measurements are larger in the data than in the theory. I was wondering if, in your opinion, this could be corrected by obtaining more accurate parton distributions, or maybe there are some missing charmonium processes, or if this should be corrected by NLO QCD?

Robert Hirosky: I think the recent work in resummation and fragmentation functions that was mentioned in Thomas Gehrmann's talk holds some promise and it will be interesting to first see the effects of these improvements. For example, the b-jet production cross section is typically compared to calculations for b quarks. Thus, fragmentation effects must be well understood. Resummation effects are also important due to the two scales in the problem. In this case we have a jet of a certain p_T and a muon with a second p_T scale defined relative to the jet. So I consider work in these two areas to be well motivated.